European Congress on Computational Methods
in Applied Sciences and Engineering (ECCOMAS 2012)
J. Eberhardsteiner et.al. (eds.)
Vienna, Austria, September 10-14, 2012

MULTIPHYSICS COMPUTATIONAL MODELS FOR CARDIAC FLOW AND VIRTUAL CARDIOGRAPHY

Jung Hee Seo[1], Vijay Vedula[1], and Rajat Mittal[1]

[1] Johns Hopkins University
3400 N Charles St, Baltimore, MD, 21218, USA
mittal@jhu.edu

Keywords: hemodynamics, hemoacoustics, echocardiography, phono-cardiography, computational fluid dynamics, Doppler ultrasound, hypertrophic cardiomyopathy, systolic murmur

Abstract. *We propose a multiphysics simulation approach for predicting cardiac flows as well as conducting virtual echo (ECHO)- and phono-cardiography (PC) of these flows. Intraventricular blood flow is simulated by solving the three-dimensional incompressible Navier-Stokes equations with an immersed boundary method. Using this computational hemodynamic data, echo- and phono cardiographic signals are synthesized by separate simulations that model the physics of ultrasound wave scattering and flow-induced sound, respectively. For virtual ECHO, a Doppler ultrasound image is reproduced through Lagrangian particle tracking of red blood cells and application of sound wave scattering theory. For virtual PC, the generation and propagation of blood-flow induced sounds is directly simulated by a computational hemo-acoustics model. The virtual ECHO is applied to reproduce an M-mode Doppler image for the left ventricle and the virtual PC is used to model systolic murmurs caused by hypertrophic cardiomyopathy(HCM). This "virtual" cardiography analysis provides data that can be compared and verified directly against clinically acquired data. Also the development of detailed correlations between blood-flow dynamics and the cardiographic data is expected to provide valuable information for the improvement of diagnostic tools based on these modalities.*

1 INTRODUCTION

Computational modeling has increasingly become the tool of choice for studying cardiac flow patterns [8,14,25,26,27,32]. The computational hemodynamics enable a comprehensive analysis of flow, pressure, vorticity and viscous dissipation in normal as well as diseased hearts, and in doing so, may reveal the significance of flow structures on ventricular function. The future of computational hemodynamics for the cardiac flows is simulation with patient specific models (e.g. [14,26]) and will eventually assist with the diagnosis and treatment of heart disease.

A number of issues and challenges exist in order to achieve this promise of computational hemodynamics of cardiac flows. This paper deals with two of these challenges: the first one is the need for method to rapidly assess the validity of the computational result for a patient specific model simulation. Although computational modeling for the cardiac flow simulations can be validated and verified for canonical (benchtop) models, this does not guarantee the validity of the computational result for a particular patient specific model simulations. This is primarily because the input data (such as inflow/outflow conditions) obtained from the patient specific measurements for the simulation oftentimes are limited and some of these need to be estimated or modeled. Thus, the overall accuracy of the computational result for a patient-specific model needs to be checked prior to using the simulation data for diagnosis and treatment. The second issue addressed here is the connection between the computational hemodynamic results and the diagnostic data used in the clinical field. Though the flow features and vortical structures can be investigated in detail with the computational hemodynamics, that information is hard to be used directly for the diagnosis and treatment for the heart diseases. Therefore for the better interpretation of the computational hemodynamic result and to find the clinical implication of hemodynamic features, it may be important to find a clear correlation between the detailed cardiac flow structures and the clinical data that are used for the cardiac diagnosis.

The above two issues can be addressed by making virtual cardiographies using the computational hemodynamic results of cardiac flows. In this study, we describe a multiphysics simulation approach for the modeling of cardiac flows as well as virtual echo- and phono-cardiography. Cardiac echocardiography (ECHO) employs Doppler ultrasound for the assessment of intracardiac flows (e.g.[4,20,28]) and phono-cardiography (PC) employs recording and analysis of heart sounds for auscultation[1,9,18,24]. Both ECHO and PC are non-invasive and inexpensive diagnostic methods for cardiac disease. Thus virtual ECHO and PC will serve as a bridge between the clinical, diagnostic data and computational hemodynamic results. In the present study, intraventricular blood flows are simulated via computational fluid dynamics (CFD), and echo- and phono-cardiographic data are synthesized by separate simulations that model the physics of ultrasound wave scattering and flow-induced sound, respectively. These "virtual" ECHO and PC provide data that can be compared directly to clinically acquired data, and improve our ability to interpret the cardiac flow simulation data. Also the development of detailed correlations between blood-flow dynamics and the cardiographic data will provide valuable information for the improvement of diagnostic tools based on these modalities. The salient features of the simulation methods are described in the following section, and in the sections following that, we demonstrate the modeling of color M-mode as well as the systolic ejection murmur associated with hypertrophic cardiomyopathy.

2 METHODS

In the present study, intraventricular blood flow is simulated by solving the three-dimensional incompressible Navier-Stokes equations with an immersed boundary method[15].

Using this computational hemodynamic result, virtual echo- and phono- cardiographies are generated via separate simulations which model the physics of ultrasound wave scattering and flow induced sound, respectively. For virtual ECHO, we reproduce a Doppler ultrasound image which depicts intraventricular flow motions. This is done by Lagrangian particle tracking of red blood cell(RBC) and applying sound wave scattering theory[22]. The motion of RBC particles is tracked by using the time-dependant Eulerian velocity field obtained from the cardiac flow simulation and ultrasound wave propagation and scattering by RBC particles are described by an acoustic analogy for arbitrary transducer/receiver shape. Once the time series of scattered ultrasound signal is obtained on the receiver, a Doppler ultrasound image can be constructed by a signal processing approach. For virtual phonocardiography, we simulate the blood flow-induced sound generation and propagation using a computational hemo-acoustics modeling approach which employs the incompressible Navier-Stokes/linearized perturbed compressible equations (LPCE) hybrid method[29]. The sound source term is obtained from the computational hemodynamic simulation results and the sound propagation through the thorax is modeled with a structural wave equation.

2.1 Computational hemodynamics

For the intraventricular blood flows, blood is assumed to be a Newtonian fluid and thus its motion is governed by the incompressible Navier-Stokes equations;

$$\nabla \cdot \vec{U} = 0, \quad \frac{\partial \vec{U}}{\partial t} + (\vec{U} \cdot \nabla)\vec{U} + \frac{1}{\rho_0}\nabla \vec{P} = \nu_0 \nabla^2 \vec{U}\,, \tag{1}$$

where $\vec{U}$ is a velocity vector, P is a pressure, ρ_0 and ν_0 are the density and kinematic viscosity of the blood. Equations (1) are solved by a projection method based approach[6]. The momentum equation is computed by a second-order Crank-Nicolson method and the pressure Poisson equation is solved by a geometric multi-grid method. All the spatial derivatives are discretized by a second-order central differencing. The discretized equations are solved on the non-body conformal Cartesian grid and the complex, moving boundaries are treated by a sharp-interface immersed boundary method as described in Ref.[15]. In this method, the endocardial surface is represented by an unstructured mesh with triangular elements and this surface is immersed into the Cartesian volume grid. In the current study, the endocardial surface moves with a prescribed velocity and the boundary conditions for the flow field on the surface are imposed by a multi-dimensional ghost cell method. Further detailes of the methodology can be found in the Ref.[15].

2.2 Blood cell particle tracking

The motion of 'virtual' red blood cells(RBC) is simulated by the Lagrangian particle tracking algorithm. The particles that represent the RBC are randomly distributed in the blood flow domain and their motion is tracked by the equation;

$$\vec{x}_p(t+\Delta t) = \vec{x}_p(t) + \int_t^{t+\Delta t} \vec{U}(\vec{x}_p)\, dt\,, \tag{2}$$

where $\vec{x}_p$ is the particle position vector and $\vec{U}(\vec{x})$ is the Eulerian velocity vector field obtained from the full Navier-Stokes computation. The velocity at the particle poistion is computed by a tri-linear interpolation and the time integration in Eq. (2) is performed by a four-stage Runge-Kutta method.

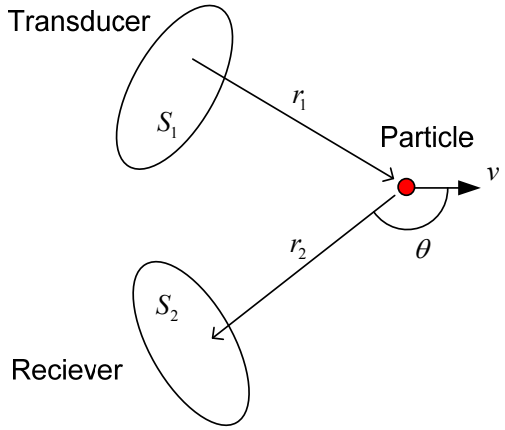

Figure 1: Schematic of Doppler ultrasound modeling.

2.3 Doppler ultrasound modeling

In this study, we model the scattering of ultrasound wave by each RBC as proposed by Oung and Forsberg[22]. As depicted in the schematic in Fig. 1, the ultrasound wave emitted from the transducer surface (S_1) propagates to the moving RBC particle and the wave scattered by the particle is received by the recevier surface (S_2). Note that two surfaces S_1 and S_2 can be the same. If we assume the sound wave is reflected spherically by the rigid small particle, the signal received at the reciever surface is given by the reciprocity[22] as;

$$s_n(t) = \frac{R}{(2\pi)^2}\int_{S_2}\int_{S_1}\frac{1}{r_2(\mu)}\frac{1}{r_1(\mu)}e(\mu - r_1(\mu)/c)\,dS_1\,dS_2, \tag{3}$$

where s_n is the signal recevied by the receiver surface for a single particle, r is the distance from the point on the transducer/receiver surfaces to the particle, c is the speed of sound, and $e(t)$ is the surface normal velocity fluctuation signal on the transducer, $\mu = t - r_2/(c - v\cos\theta)$, and R is a constant reflection coefficient.

The Doppler signal can be produced by performing a direct sampling[22] of received signal $s_n(t)$ at $t_s=t_g+kT$, where t_s is the sampling time, t_g is the sampling start time, k is an integer, and T is the peroid of original signal, $e(t)$. Also in order to add phase information on the sampled signal, a complex signal[22], $\tilde{s}_n(t_s)$ can be constructed by replacing $e(t)$ in Eq. (3) with $\tilde{e}(t) = e(t) + ie'(t)$, and $e'(t)$ is the Hibert transform of $e(t)$. The Fourier transform of $\tilde{s}_n(t_s)$ gives the frequency shift associated with theparticle velocity. The received signal for all the RBC particles in the blood volume can be obtained by

$$\tilde{s}(t_s) = \sum_{n=1}^{N}\tilde{s}_n(t_s), \tag{4}$$

where N is the total number of particles. Here we neglected the effect of multiple scattering by assuming R is small (i.e. weak scattering). The frequency analysis of $\tilde{s}(t_s)$ gives the velocity information of the target blood volume and this is the basis of the Doppler ultrasound image construction. In this study, the transducer/receiver surface is represented by triangular surface meshes and the surface integrals in Eq. (3) are evaluated by using the trapzoidal rule.

2.4 Computational hemo-acoustics

The sound generated by blood flow in the heart is simulated with an immersed boundary method based hybrid approach. First, the hemodynamic flow field inside the heart is simulated with the immersed boundary incompressible Navier-Stokes flow solver described above, and the flow-induced sound generation and propagation are modeled by the linearized per-

turbed compressible equations (LPCE) [29]. The incompressible Navier-Stokes/LPCE hybrid method is a two-step, one-way coupled approach for the prediction of flow induced sound at low Mach numbers [17,29,30]. Since the heart sound is generally auscultated on the chest (precordium) surface, the sound propagation through the thorax is also modeled by a linear structural wave equation. The LPCE and a linear wave equation are fully coupled by combining them into a single set of equations and, the different material domains are treated by varying the material properties. A unified single set of acoustic equations are written as

$$\begin{aligned} &\frac{\partial \vec{u}'}{\partial t} + H(\vec{x})\nabla(\vec{u}\cdot\vec{U}) + \frac{1}{\rho(\vec{x})}\nabla p' = 0, \\ &\frac{\partial p'}{\partial t} + H(\vec{x})\left[(\vec{U}\cdot\nabla)p' + (\vec{u}'\cdot\nabla)P\right] + K(\vec{x})(\nabla\cdot\vec{u}') = -\frac{DP}{Dt}H(\vec{x}), \end{aligned} \tag{5}$$

where ($'$) represents the compressible (acoustic) perturbation, H is a Heaviside function which has a value of 1 in the blood flow region and 0 elsewhere, and the density (ρ) and bulk modulus ($K=\rho c^2$) are functions of space [31]. The capital letters (U,P) indicates the hydrodynamic incompressible variables and they are obtained from the incompressible flow simulations. By solving Eqs. (5), the wave transmission and reflection at the interface between the blood flow and tissue are automatically resolved based on the difference of acoustic impedance $Z=K/c$. In this model the propagation of shear waves in the tissue material is not considered, since the shear modulus of the tissue materials is much smaller than the bulk modulus[21]. Also the dissipation of the acoustic wave is neglected since the frequency range of the heart sound is typically low (~O(100) Hz) and the dissipation for these low frequencies is expected to be very small. The current fluid-like assumption of the tissue material for the purpose of resolving acoustic wave propagation has been widely used for the simulation of sound wave propagation in biological materials[2,19,21]. The present approach has also been used for the direct computation of arterial bruits sound[31]. Equations (5) are spatially discretized with a fourth-order compact finite difference scheme[13] and integrated in time using a four-stage Runge-Kutta method. A second-order Lagrangian interpolation[30] is used for the temporal interpolation of flow variables.

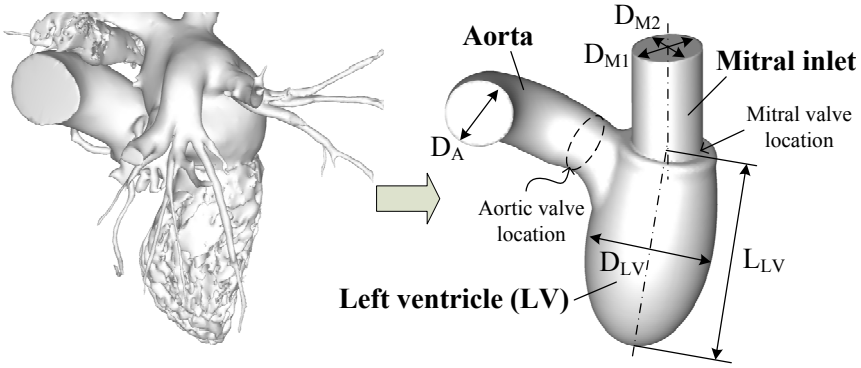

Figure 2: Three dimensional model of the left ventricle. Left: real left venticle model extracted from the contrast CT scan. Right: a simplified model used for the intraventricular flow simulation.

3 RESULT AND DISCUSSION

3.1 Left ventricle model

We have constructed a simplified model of the left ventricle (LV) based high-resolution, multi-detector contrast CT scan of the LV. Figure 2 shows the model and some geometrical parameters. In this study we use: D_{M1}=2.4 cm, D_{M2}=2.0 cm, D_A=2.0 cm, D_{LV}=3.75 cm,

L_{LV}=6.5 cm, and the end-systolic ventricle volume is 56 ml. Although the mitral and aortic valve motions are not simulated, we mimic the opening and closure of those valves by changing the geometry of the LV model for the diastole and systole phases. For the diastole phase, the aorta is blocked at the aortic valve location, while the mitral inlet is blocked at the mitral valve location during the systole phase. The blood volume flow rate through the mitral inlet (diastole) or the aorta (systole) is modeled based on the previous study[33]. The generic blood flow rate profile is shown in Fig. 3. Here negative value of flow rate is for the blood coming through the mitral inlet and positive value is for the blood ejected to the aorta. In this study, the heart rate is assumed to be 60 BPM (i.e. the duration of one heart cycle is 1 sec), and we use the following parameters; Q_E=314 ml, Q_A=0.5Q_E, t_{EE}=0.3 sec, t_{AS}=0.45 sec, t_{AE}=0.64 sec, t_{SS}=0.68 sec, t_{SP}=0.78 sec, and t_{SE}=0.98 sec. These parameters yield the ejection fraction, EF=53%, and the E/A ratio based on the peak volume averaged velocity is 2. This E/A ratio corresponds to the 'restrictive filling' case[23]. The LV motion (expansion and contraction) is prescribed by satisfying the volume flow rate.

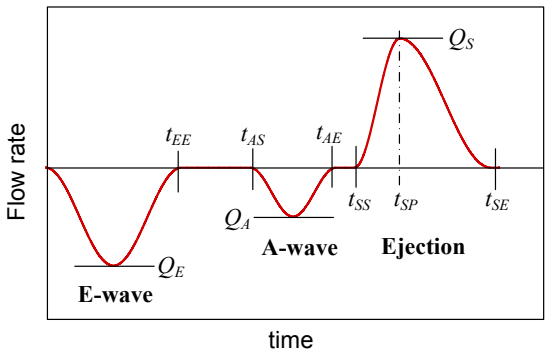

Figure 3: A blood flow rate model for the left ventricle.

3.2 Intraventricular hemodynamics

The above LV model is represented by the unstructured surface mesh of 37256 triangular elements and this surface mesh is immersed on the Cartesian volume mesh of 256×256×384 (25M) for the high-resolution simulation of the intraventricular flow. At the boundaries of inlet (mitral inlet) and exit (aorta), the pressure is specified and the zero-normal-gradient condition is applied for the velocities. At the exit boundary, we use the back-flow-stabilization boundary condition suggested by Moghadam et al.[16] and on the ventricular wall, a no-slip, no-penetration boundary condition is applied. For the present case, the Reynolds number based on the mitral inlet diameter (D_{M1}) and the peak volume averaged velocity through the mitral inlet is about 4000. The intraventricular flow fields obtained by solving Eq. (1) are visualized in Figs. 4 and 5.

Figure 4 shows the time evolution of vortical structure during the diastole stage. At t=0.2 sec, a vortex ring generated by the incoming blood flow of E-wave (Fig. 3) is clearly observed. The vortex ring is slightly tilted in counter-clockwise direction, since the convection speed of the right hand side of the vortex ring is slowed down by the interaction with the lateral wall of the ventricle. Due to this interaction with the wall and the relatively high Reynolds number , the vortex ring quickly becomes unstable and starts to breakdown(0.3 sec). The vortex ring is completely broken into small eddies and the local flow shows signs of turbulence (0.4 sec). The small eddies are also observed to dissipate rapidly. At 0.6 sec, another but weaker vortex ring is generated by the incoming flow associated with the A-wave.

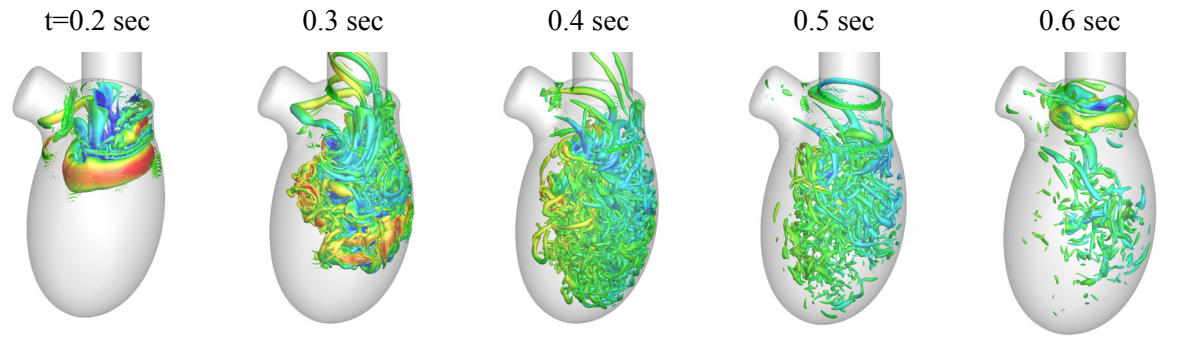

Figure 4: Time evolution of intraventricular vortical structure during the diastole stage. Vortical structure is visualized by Q-criteria (iso-surface of Q=20000 sec^{-2}) and colored by the axial (along the center line of mitral inlet) velocity.

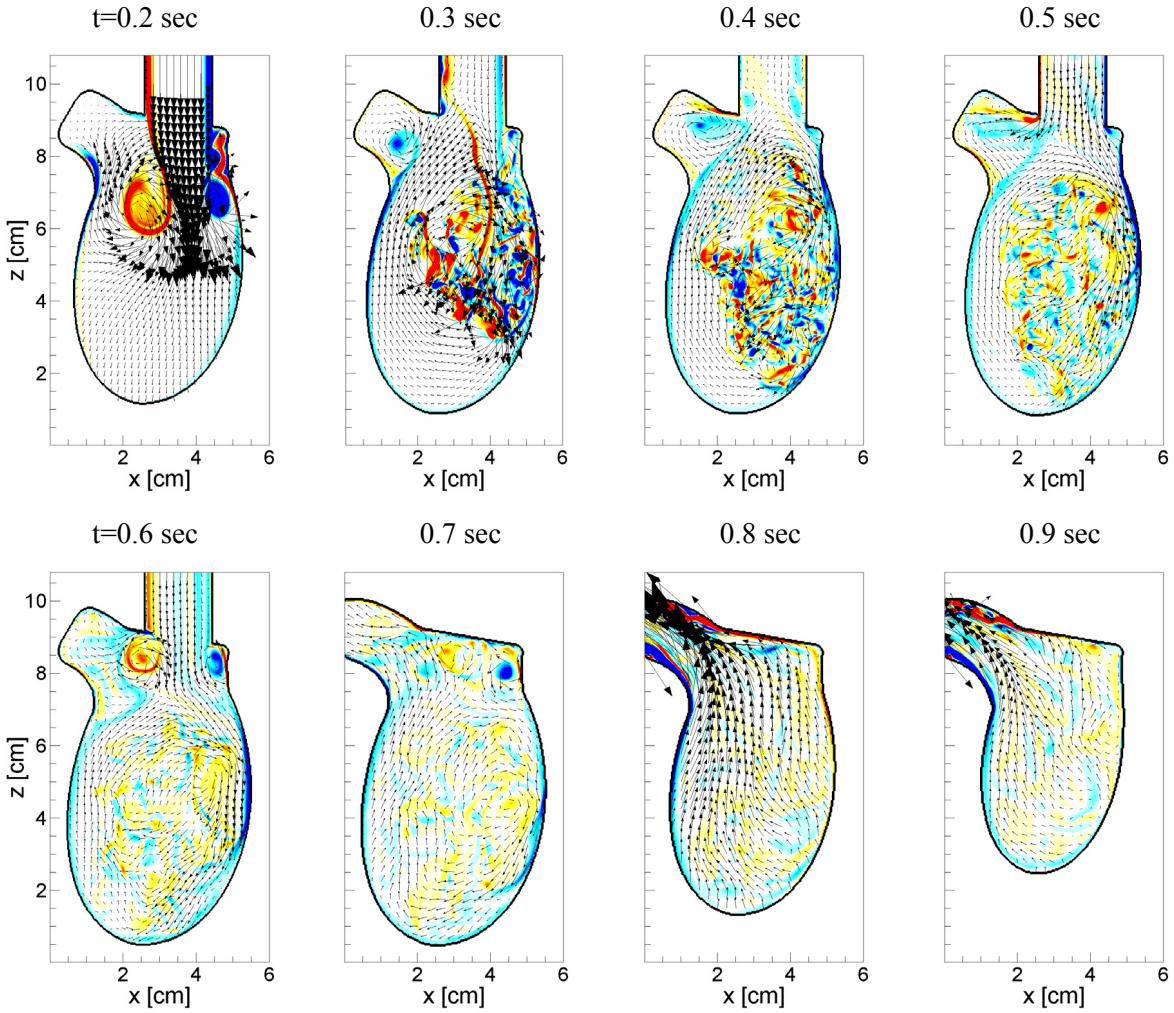

Figure 5: Vorticity contours and velocity vectors at the cross-section for whole heart cycle. Color contour denotes y-component vorticity and the every 8th vectors are plotted.

The flow patterns in the ventricle are visualized in Fig. 5 by the vorticity contours and velocity vectors on the long-axis plane for whole heart cycle. At t=0.2 sec, one can see that the right hand side vortex is decaying due to the interaction with the wall, while the left hand side vortex becomes dominant. Thus the vortical flows move toward the lateral wall, and the overall intraventricular flow exhibits a clockwise circulation. The E-wave vortex breaks and dissipates during the diastole (0.3-0.5 sec). The incoming flow of the A-wave goes primarily to the

lateral wall by the interaction with the clockwise circulation and small vortex ring is formed near the mitral annuals during the deceleration of A-wave (t=0.6 sec). The overall clockwise circulation pattern is still observed during early systole (0.7 sec), and due to this, the velocity strength near the septal wall is bit stronger during the ejection. The overall intraventricular flow pattern is similar to the results of previous studies[7,12,27,32,33] but, by using a high-resolution computational grid, we observe smaller scale flow structures that are not reported previously.

3.3 Virtual red blood cell particle tracking

The red blood cell (RBC) motions are modeled via Largrangian particle tracking and the obtained RBC motions are used for the Doppler ultrasound simulation. Initially, a total of 6000 particles that represent the RBC groups are randomly distributed in the blood flow domain, and the particle motion is computed by Eq. (2). The particles are continuously injected though the mitral inlet during the diastole, and the particles exiting the aorta during the systole are eliminated from the simulation. The position and velocity of each RBC particle are saved for the Doppler ultrasound computation.

3.4 Doppler ultrasound simulation

A color M-mode[4] image is produced by a pulsed wave (PW) Doppler ultrasound. For the ultrasound wave simulation, we employed a transducer/receiver (transducer hereafter) of parabolic shape. The size of the transducer is 2 cm and the distance to the focus point of the parabola is 3 cm. The transducer surface is discretized by 160 triangular elements for the computation and the main driving frequency of ultrasound is 2 MHz. The transducer is located at the center of mitral inlet and 11 cm below from the mitral valve location. The direction of ultrasound wave beam is perfectly aligned with the mitral inlet axis (z-dir). The pulse duration is 1 μsec and the pulse repeating frequency (PRF) is 10 kHz. At a given time, PW scans the blood volume located at the specific distance (d) from the transducer. If we sample the received signal at the PRF, the distance, d, is related with the sampling start time, t_g, by $d=t_g c/2$. On the spectrograms of sampled signals, one can find the representative velocity of the blood volume at the given distance (d) and time (t) based on the maximum energy level of the spectrogram, and consequently construct the velocity field in a 2D space, i.e. $V(t,d)$. A color M-mode cardiogram can be made by plotting this velocity field with color contours in a 2D space.

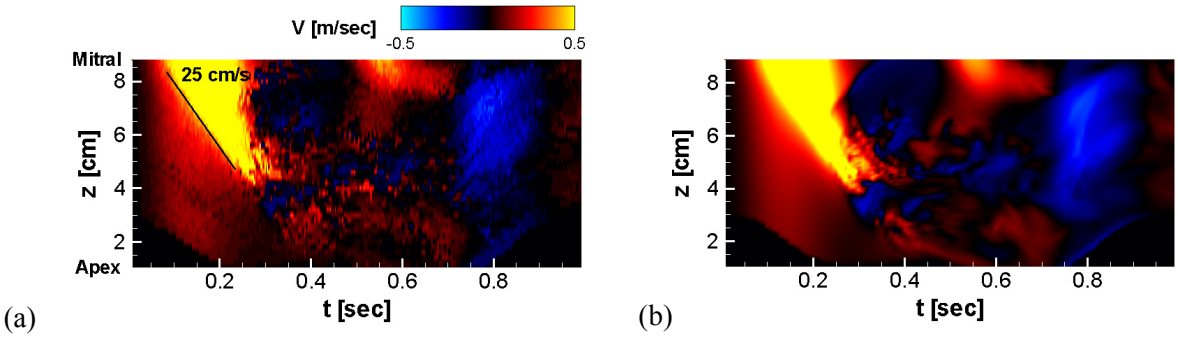

Figure 6: Temporal velocity variation along the mitral center line. (a) Simulated color M-mode Doppler image. (b) Data obtained directly from the flow field simulation.

The velocities in a total of 40 sample volumes from the apex to the mitral valve position are evaluated and the spatial resolution of sampling is 2 mm. The resulting color M-mode image is shown in Fig. 6(a). Here a positive velocity implies motion toward the transducer, i.e.

direction to the apex. Figure 6(b) shows the similar plot made by using the z-direction velocity values directly obtained from the flow field computation and it shows very good correlation with the M-mode Doppler plot. In Fig. 6(a), one can see the propagation of blood flow which comes into the ventricle with E and A waves. The propagation velocity of blood flow is usually evaluated by the slope of the velocity contour on the color M-mode image and used as a parameter to estimate the ventricle function. In the present case, the propagation velocity for the E-wave is about 25 cm/sec (solid line in Fig. 6(a)) which is in the physiological range[4]. However, a proper way to determine this propagation velocity is still arguable[5]. With the current computational hemodynamics and Doppler ultrasound simulation approach, it is possible to investigate the correlation between the evaluated propagation velocity and the actual blood transportation velocity, and this will be pursued in the future study.

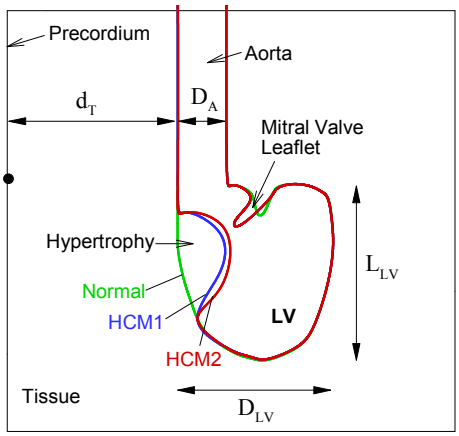

Figure 7: Schematic of simplified left ventricle model with hypertrophy for the computation of systolic ejection murmur.

3.5 Simulation of systolic ejection murmur

Heart sound contains important information regarding the health of the cardiac system and auscultation can therefore be used as a non-invasive diagnostic modality for the heart disease. Heart sound may be recorded using an electro-stethoscope and the resulting phonocardiogram is analyzed for detection of abnormal heart sounds associated with heart disease[9]. In the current study, we predict the generation of abnormal heart sound through direct computation of flow and sound and use this to generate a virtual phonocardiogram. In particular, we consider here a systolic ejection murmur caused by a hypertrophic cardiomyopathy (HCM). It is generally believed that the systolic ejection murmur is generated by the blood flow disturbances due to an obstruction in left-ventricular outflow tract (LVOT)[1]. In the present study we compute this blood flow induced sound generation and propagation.

A simplified model of two-dimensional cross section of the left ventricle with ascending aorta is constructed to simulate the hemodynamic flow field during the systole and associated murmurs (Fig. 7). Here D_A=2 cm, d_T=7cm, D_{LV}=6.4 cm, and L_{LV}=7.4 cm (at the beginning of systole). A sub-aortic, obstructive hypertrophy is modeled as shown in Fig. 7 for HCM cases. In addition to a normal case, we considered two HCM cases, HCM1 and HCM2, and HCM2 has more severe hypertrophy than HCM1. For the HCM cases, the mitral valve leaflet is elongated and moved toward the outflow tract to mimic systolic anterior motion (SAM) which manifests in many severe cases of HCM. In the present study, however, a dynamic motion is not considered and it is assumed that two HCM cases have the same degree of SAM. The re-

sulting gap size in the outflow tract is about $0.3D_A$ for HCM1 and $0.2D_A$ for HCM2. The simulations are performed for only systole phase and the systole time (t_{ES}-t_{SS}) of 0.25 sec is used here. The blood flow domain inside the LV and aorta is resolved by 256 × 384 non-uniform Cartesian grid with the minimum grid spacing of $0.015D_A$.

The acoustic domain includes the LV and aorta as well as nearby thorax region represented by a box in Fig. 7. The acoustic computation is performed on the separate grid which consists of 200×200 grid points with a minimum grid spacing of $0.04D_A$. The flow simulation results are interpolated onto the acoustic grid in the LV and aorta region using a bi-linear interpolation. The density and speed of sound for the blood are set to 1.05 (g/cm^3) and 1500 (m/s), respectively. For the present simplified thorax model, a thoracic region outside the heart is assumed consist of a homogeneous tissue material and its density and speed of sound are assumed to be 1.2 (g/cm^3) and 1800 (m/s). These values are averaged material properties of various components in the thorax[10]. The left boundary of the acoustic domain represents the precordium surface and the heart sound is monitored there as is done in the actual auscultation. Since a stethoscope senses transmitted sound via the velocity (or acceleration) of the chest surface[3], we have recorded the velocity fluctuations on the monitoring points shown in Fig. 7. The zero-stress boundary condition is applied at the precordium surface and it is assumed that acoustic waves radiate through all other boundaries.

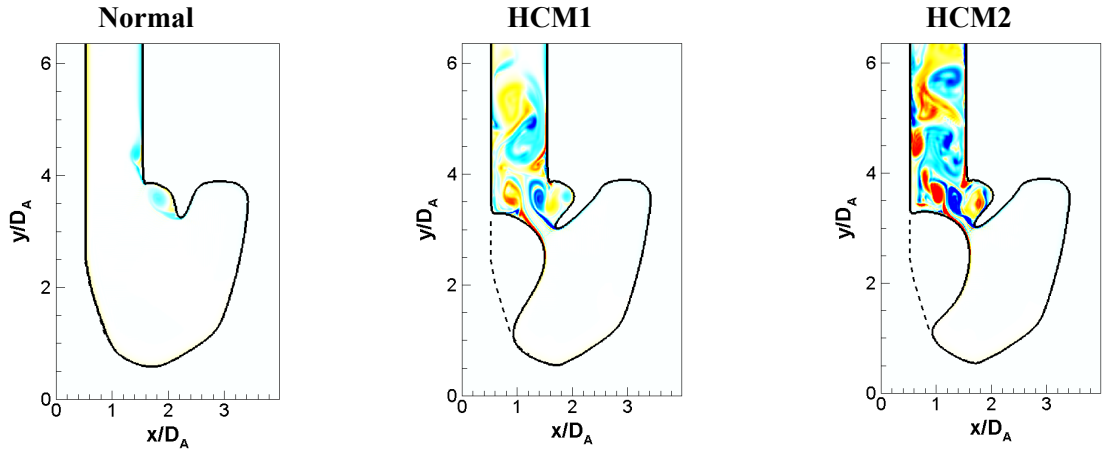

Figure 8: Instantaneous hemodynamic flow field for the normal and HCM cases represented by vorticity contours at t = 0.13 sec (t=0 is the start of systole phase).

The instantaneous hemodynamic flow fields for normal, HCM1, and HCM2 cases are shown in Fig. 8 with the vorticity contours. For normal case, there is no significant vortex motions in the LVOT and aorta. With hypertrophy and SAM, however, the formation of a jet in the gap between the hypertrophy and the mitral valve leaflet is observed and the jet shear layer rolls into vortices which interact with the aortic wall. This complex vortex motion is supposed to be the source of murmur sound. For the smaller gap (HCM2), the blood flow velocity through the gap becomes faster and exhibits stronger vortex motions.

The acoustic fields are computed by Eq. (5) using the hemodynamic flow field results. The velocity fluctuations monitored on the precordium surface are plotted in Fig. 9 for HCM1 and HCM2 cases. For the normal case, no significant velocity fluctuation is observed. Figure 9 is the recorded murmur signal for the cases with HCM and can be considered as a virtual phonocardiogram for the HCM murmur. The present simulated murmur signal exhibits a crescendo/descendo configuration[1] (especially for HCM2) which is quite common in systolic

murmurs. Note that, with larger hypertrophy (HCM2), much stronger murmur sound is generated.

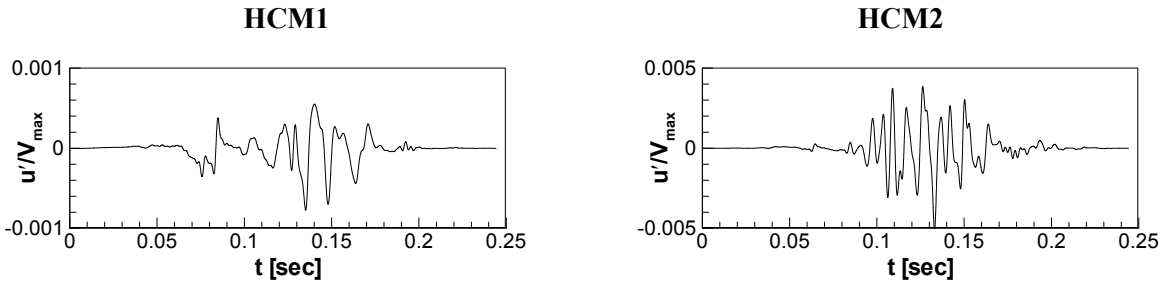

Figure 9: Acoustic velocity fluctuation monitored on the precordium surface. Time signal band-pass filtered for 20-400 Hz.

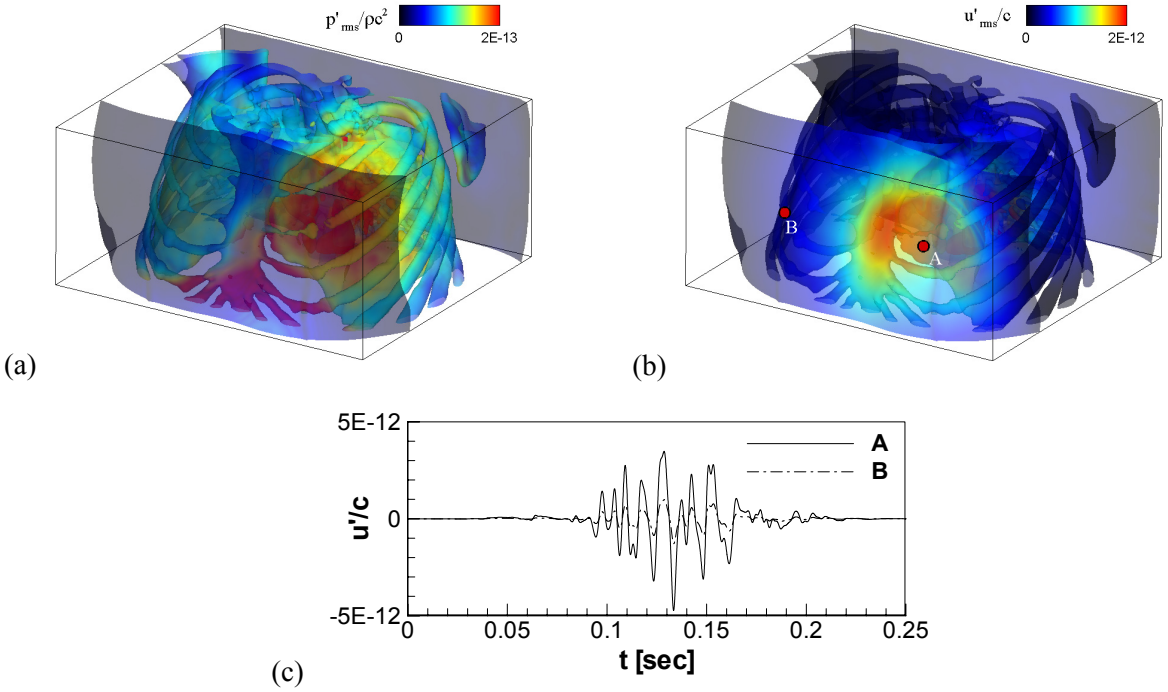

Figure 10: Propagation of systolic HCM murmur computed with a realistic human thorax model. (a), (b) Root-mean-squared acoustic pressure and velocity fluctuations plotted on the density iso-surfaces. (c) Phonocardiac signals for the HCM systolic murmur monitored on the points A and B in figure (b). The signals are band-pass filtered for 20-400 Hz. Here ρ and c are the density and the speed of sound of the blood.

Now in order to examine the effect of heart sound propagation in a real human thorax which includes many different biological materials such as chest bones and lungs, we have considered a three-dimensional realistic human thorax model. The model is constructed based on the Visible Human®[1] Dataset. For the simulation of sound propagation, the contrast value on the CT scan images is converted to the material density and the speed of sound using the formulation proposed in Ref.[19]. For the sound source, we use DP/Dt value on the left ventricle obtained from the hemodynamic flow field simulation of HCM2 case, and this source term is placed on the left ventricle position of the constructed real thorax model. Figure 10(a)

[1] An anatomical data set developed under a contract from the National Library of Medicine by the Departments of Cellular and Structural Biology, and Radiology, University of Colorado School of Medicine

and (b) show the root-mean-squared acoustic fields of HCM murmur radiated in the realistic thorax model. One can clearly see the high pressure fluctuation around the heart location and high velocity fluctuation on the chest surface above the heart. The velocity fluctuations are monitored on the two locations A and B shown in Fig. 10(b) and plotted in Fig. 10(c). Figure 10(c) is thus the virtual phonocardiogram of HCM murmur predicted with the realistic thorax model. The point A is on the chest surface directly above the heart, thus the signal monitored at this point shows higher amplitude than point B. Interestingly, the signal monitored at point A looks very similar with the result of simplified thorax model shown in Fig. 9(HCM2).

The present coupled computational hemodynamic-hemoacoustic approach for the virtual phonocardiogram can be used for a comprehensive investigation of the heart sound generation mechanism and it has the potential to improve the diagnostic ability of the cardiac auscultation. The present method will also be applied to the third and fourth heart sounds[24] to reveal the generation mechanism of those abnormal heart sounds.

4 CONCLUSION

In this study, multi-physics simulation methods are presented for the simulation of intraventricular blood flows, Doppler ultrasound, and blood flow induced heart sounds. The reconstruction of color M-mode Doppler and the simulation of systolic HCM murmur are demonstrated. These virtual cardiographic data not only provide new ways for interpreting computational hemodynamic results but also allow us to investigate the correlation between the diagnostic data and the cardiac blood flow dynamics. The development of such correlations will provide valuable information such as disease-diagnostic data-associated cardiac flow feature relation and this will help the diagnosis and treatment of specific heart diseases.

ACKNOWLEDGEMENT

This research is supported by the CDI program at NSF through grant IOS-1124804. This work used the Extreme Science and Engineering Discovery Environment (XSEDE), which is supported by NSF grant number TG-CTS100002. The Visible Human® Dataset was provided by the National Library of Medicine. The authors also thank Dr. Albert C. Lardo for providing the contrast CT scan data.

REFERENCES

[1] M. A. Alpert: Systolic murmurs, In H.K. Walker, W.D. Hall, J.W. Hurst, editors, Clinical Methods:The History, Physical, and Laboratory Examinations. 3rd Ed. Boston:Butterworths (1990), Chapter 2.

[2] C. Baron, J.-F. Aubry, M. Tanter, S. Meairs, M. Fink M: Simulation of intracranial acoustic fields in clinical trials sonothrombolysis, *Ultrasound Med Biol*, 35(7) (2009), 1148-1158.

[3] A.O. Borisyuk: Noise field in the human chest due to turbulent flow in large blood vessel, *Flow Turbul Combust*, 61(1999), 269-284.

[4] J. M. Carcia, N. G. Smedira, N. L. Greenberg, M. Main, M. S. Firstenberg, J. Odabashian, J. D. Thomas: Color M-mode Doppler flow propagation velocity is a preload in-

sensitive index of left ventricular relaxation: animal and human validation, *J.Am.Coll.Cardiol*. 35 (2000), 201–208.

[5] N. Casandra, O. Takahiro, V. Pavlos, L. William: Measuring heart filling propagation velocity using the cross wavelet transform, 64th Annual Meeting of the APS Division of Fluid Dynamics, November 20-22, 2011, abstract #D13.002.

[6] A.J. Chorin: On the convergence of discrete approximations to the Navier–Stokes equations, *Math. Comput.* 23(106) (1969), 341–353

[7] T. Doenst, K. Spiegel, M. Reik, M. Markl, J. Henning, S. Nitzsche, F. Beyersdorf, H. Oertel: Fluid-dynamics modeling of the human left ventricle: methodology and application to surgical ventricular reconstruction, *Ann. Thorac. Surg*. 87 (2009), 1187–1195.

[8] F. Domenichini, G. Pedrizzetti, B. Baccani: Three-dimensional filling flow into a model left ventricle, *J.Fluid Mech.* 539 (2005), 179–198.

[9] P. Erne: Beyond auscultation - Acoustic cardiography in the diagnosis and assessment of cardiac disease, *Swiss Med Wkly*, 138(2008), 439-452.

[10] S.A. Goss, L. A. Frizzell, F. Dunn F: Dependence of the ultrasonic properties of biological tissue on constituent proteins, *J Acoust Soc Am*, 67(3) (1980),1041-1044.

[11] J. A. Jensen, N. B. Svendsen, Calculation of pressure fields from arbitrarily shaped, apodized, and excited ultrasound transducers, *IEEE Trans Ultrasonics Ferroelectrics and Frequency control*, 30(1992), 262-267.

[12] P. J. Kilner, G. Yang, A. J. Wilkes, R. H. Mohiaddin, N. Firmin, M. H. Ycoub: Asymmetric redirection of flow through the heart, *Nature Letter* 404 (2000), 759–761.

[13] S. K. Lele: Compact finite difference schemes with spectral-like resolution, *J Comput Phys* 103(1992),16-42.

[14] V. Mihalef, R. Ionasec, P. Shuarma, B. Georgescu, I. Voigt, M. Suehling, D. Comaniciu: Patient-specific modelling of whole heart anatomy, dynamics and hemodynamics from four-dimensional cardiac CT images, *Journal of the Royal Society Interface Focus* 1 (2011), 286–296.

[15] R. Mittal, H. Dong, M. Bozkurttas, F.M. Najjar, A. Vargas, A.A. von Loebbecke: A versatile sharp interface immersed boundary method for incompressible flows with complex boundaries. *Journal of Computational Physics*, 227(2008),4825-4852.

[16] M. E. Moghadam, Y. Bazilevs, T.-Y. Hsia, I. E. Vignon-Clementel, A. L. Marsden: A comparison of outlet boundary treatments for prevention of backflow divergence with relevence to blood flow simulations, *Comput Mech*, 48(2011), 277-291.

[17] Y. J. Moon, J. H. Seo, Y. M. Bae, M. Roger, S. Becker: A hybrid prediction method for low-subsonic turbulent flow noise, *Comput Fluids* 39(2010), 1125-1135.

[18] Murgo JP: Systolic ejection murmur in era of modern cardiology, what we really know? *J Am Coll Cardiol* 32(6) (1998),1596-1602.

[19] C. Narasimhan, R. Ward, K.L. Kruse, M. Gudatti, G. Mahinthakumar: A high resolution computer model for sound propagation in the human thorax based on the Visible Human data set, *Computers in Biology & Medicine*, 34(2004),177-192.

[20] R. A. Nishimura, A. J. Tajik: Evaluation of diastolic filling of left ventricle in health and disease: Doppler Echocardiography Is the Clinician's Rosetta Stone, *J Am Coll Cardiol*, 30(1997), 8-18.

[21] K. Okita, K. Ono, S. Takagi, Y. Matsumoto: Development of high intensity focused ultrasound simulator for large-scale computing*, Int J Numer Meth Fluids* 65(2010), 43-66.

[22] H. Oung, F. Forsberg: Doppler ultrasound simulation model for pulsatile flow with non-axial components, *Ultrasonic Imaging*, 18(1996), 157-172.

[23] M. M. Redfield, S. J. Jacobsen, J. C. Burnett Jr., D. W. Mahoney, K. R. Bailey, R. J. Rodeheffer: Burden of systolic and diastolic ventricular dysfunction in the community; Appreciating the scope of the heart failure epidemic, *J Am Med Assoc*, 289(2) (2003), 194-202.

[24] J. A. Jr Ronan: Cardiac auscultation: the third and fourth heart sounds, *Heart Disease and Storke*, Sep-Oct; 1(5) (1992),267-270.

[25] N. R. Saber, A. D. Gosman, N. B. Wood, P. J. Kilner, C. L. Charrier, D. N. Firmin: Computational Flow modeling of the left ventricle based on in vivo MRI data: initial experience, *Ann. Biomed. Eng.* 29 (2001), 275–283.

[26] N. R. Saber, N. B. Wood, A. D. Gosman, R. D. Merrifield, G. Yang, C. L. Charrier, P. D. Gatahouse, D. N. Firmin: Progess towards patient specific computational flow modeling of the left heart via combination of magnetic resonance imaging with computational fluid dynamics, *Ann. Biomed. Eng.* 31 (2003), 42–52.

[27] T. Schenkel, M. Malve, M. Markl, B. Jung, H. Oertel: MRI-based CFD analysis of flow in a human left ventricle methodology and application to a healthy heart, *Ann. Biomed. Eng.* 37(3) (2009), 505–515.

[28] Z. Sasson, P. G. Yock, L. K. Hatle, E. L. Alderman, R. L. Popp: Doppler echocardiographic determination of the pressure gradient in hypertrophic cardiomyopathy, *J Am Coll Cardiol*, 11(1988), 752-756.

[29] J.H. Seo, Y. J. Moon: Linearized perturbed compressible equations for low Mach number aeroacoustics, *J Comput Phys* 218(2006), 702-719.

[30] J.H. Seo, R. Mittal: A high-order immersed boundary method for acoustic wave scattering and low Mach number flow induced sound in complex geometries, *Journal of Computational Physics*, 230(2011),1000-1019.

[31] J. H. Seo, R. Mittal: A coupled flow-acoustic computational study of bruits from a modeled stenosed artery, *Medical & Biological Engineering & Computing* (2012) DOI: 10.1007/s11517-012-0917-5.

[32] H. Watanabe, S. Sugiura, H. Kafuku, T. Hisada: Multiphysics simulation of left ventricular filling dynamics using fluid-structur interaction finite element method, *Biophysical Journal*, 87(2004), 2074-2085.

[33] X. Zheng, J. H. Seo, V. Vedula, T. Abraham, R. Mittal: Computational modeling and analysis of intracardiac flows in simple models of the left ventricle, *European Journal of Mechanics - B/Fluids* 35 (2012), 31-39.